Astron. Astrophys. 117, 319–331 (1983)

ASTRONOMY AND ASTROPHYSICS

The spatial distribution and spectral characteristics of the diffuse soft X-ray background

K. P. Singh, P. C. Agrawal, R. K. Manchanda, S. Naranan, and B. V. Sreekantan

Space Physics Group, Tata Institute of Fundamental Research, Homi Bhabha Road, Bombay 400005, India

Received March 29, accepted September 20, 1982

Summary. The diffuse emission in soft X-rays (0.1–2.5 keV) was measured over half the sky with 5° (FWHM) spatial resolution during a sky survey experiment. X-ray intensity maps in galactic coordinates are presented in *B* (0.1–0.19 keV), *L* (0.1–0.28 keV), and *M* (0.4–0.9 keV) energy bands. The maps contain observations from part of the sky bounded by galactic longitudes $l=180°$ to 270° and galactic latitudes $b=40°$ to 80°, which is poorly studied in other surveys. Regions of excess soft X-ray emission are found to be associated with an edge of Loop I and its extension in the southern galactic hemisphere, the northern H I hole and other features in H I and radio continuum surveys. No quantitative correlation is observed between the X-ray intensity and natural hydrogen column density (N_H). The energy spectra observed from some regions outside the Loop I are best fitted with thermal emission spectra of a hot plasma with cosmic elemental abundances, negligible interstellar absorption and temperature $10^{6.2}$–$10^{6.3}$ K. The observed emission measures over several regions of sky are in the range of $(0.27–1.0)\,10^{-2}\,\mathrm{cm}^{-6}\,\mathrm{pc}$. Present data support the local origin for the soft X-ray background from a thermal plasma of pressure $\gtrsim 4600\,\mathrm{cm}^{-3}\,\mathrm{K}$, temperature $\sim 10^6$ K and size $\lesssim 330$ pc. A spread in the temperature of the local hot plasma with cosmic elemental abundances, is necessary to explain the observed variation in the hardness ratio.

Key words: soft X-ray background – hot interstellar medium – X-ray spectra

1. Introduction

The intensity distribution of diffuse soft X-rays in the energy range 0.1–2.0 keV has been studied for almost a decade and has covered most of the sky (de Korte et al., 1976; Hayakawa et al., 1978; Iwanami et al., 1979; McCammon et al., 1979; Fried et al., 1980; Singh et al., 1981a, b and references therein). The soft X-ray sky shows complex features with the intensity varying by a factor as large as five and the energy spectrum changing significantly over different regions of the sky.

The observed lack of absorption by the Magellanic clouds and by M 31 (McCammon et al., 1971, 1976; Long et al., 1976; Seward and Mitchell, 1981) indicates that the diffuse component of X-rays below 0.28 keV is mostly ($\gtrsim 80\%$) of galactic origin. The possible contribution of unresolved stars to the soft X-ray background has been estimated to be about 20% in the 0.28–1.0 keV energy band and $\lesssim 3\%$ in the 0.15–0.28 keV energy band, thereby supporting the non-stellar origin of the soft X-ray background (Vanderhill et al., 1975; Levine et al., 1977; Rosner et al., 1981).

The energy spectra of soft X-rays obtained from different regions of the sky can be fitted by models of X-ray emission from a hot, thin, interstellar plasma of temperature $1.5\,10^6$ K and with no significant correlation for low energy attenuation by intervening matter. This indicates a local, thermal origin of the soft X-ray background (Sanders et al., 1979; Hayakawa et al., 1978; Fried et al., 1980). This model is supported by the detection of C V, C VI, O VII, O VIII emission lines in the diffuse X-ray spectra reported by Inoue et al. (1979), Inoue et al. (1980), and Schnopper et al. (1981). The observations of the ultraviolet absorption lines of interstellar O VI (see review by Jenkins, 1977) further support the existence of hot interstellar plasma at temperatures between $3\,10^5$ K to 10^6 K. The probable energy source for heating the plasma to such high temperatures is believed to be the energy released in the supernovae explosions which can heat the interstellar matter and maintain a substantial fraction of it at a temperature 10^6 K (Cox and Smith, 1974; McKee and Ostriker, 1977; Cox, 1979, 1981).

In the present paper we report the distribution and the energy spectrum of the soft X-ray diffuse component in the energy range 0.1–2.0 keV, covering a major portion of well known radio loops – Loop I, Loop III, and Loop IV and the rather scantily studied region bounded by $l=180°$ to 270° and $b=40°$ to 80°, which has not been covered in the otherwise complete survey of Wisconsin (McCammon et al., 1979). The data are presented in the form of intensity maps in the following energy bands; 0.1–0.19 keV (*B*-band), 0.1–0.28 keV (*L*-band), and 0.4–0.9 keV (*M*-band). Correlation of the intensities in *L*- and *B*-bands with N_H, correlation of *L*-band intensity with *B*-band intensity and the galactic distribution of the hardness ratio, *R*, defined as *L*-band intensity over *B*-band intensity, are discussed in an attempt to characterize the emission regions in terms of temperature, pressure and the extent of hot plasma. The hardness ratio of *M* over *L* band intensities is not discussed in view of the significant stellar contribution to the diffuse X-ray background in the *M*-band. Spectral details are presented for a large number of broad regions outside the Loop I so as to study the spectra of diffuse X-ray background only. The spectra from some of the regions are best fitted with a single temperature ($10^{6.2}$–$10^{6.3}$ K) X-ray emitting plasma (Kato, 1976) with negligible absorption due to interstellar matter and thus supporting the local, thermal origin of the diffuse soft X-ray background. An additional higher temperature component ($T\sim 10^{6.5}$–$10^{7.0}$ K) tends to improve the fits to the spectral data in certain other directions.

Send offprint requests to: K. P. Singh

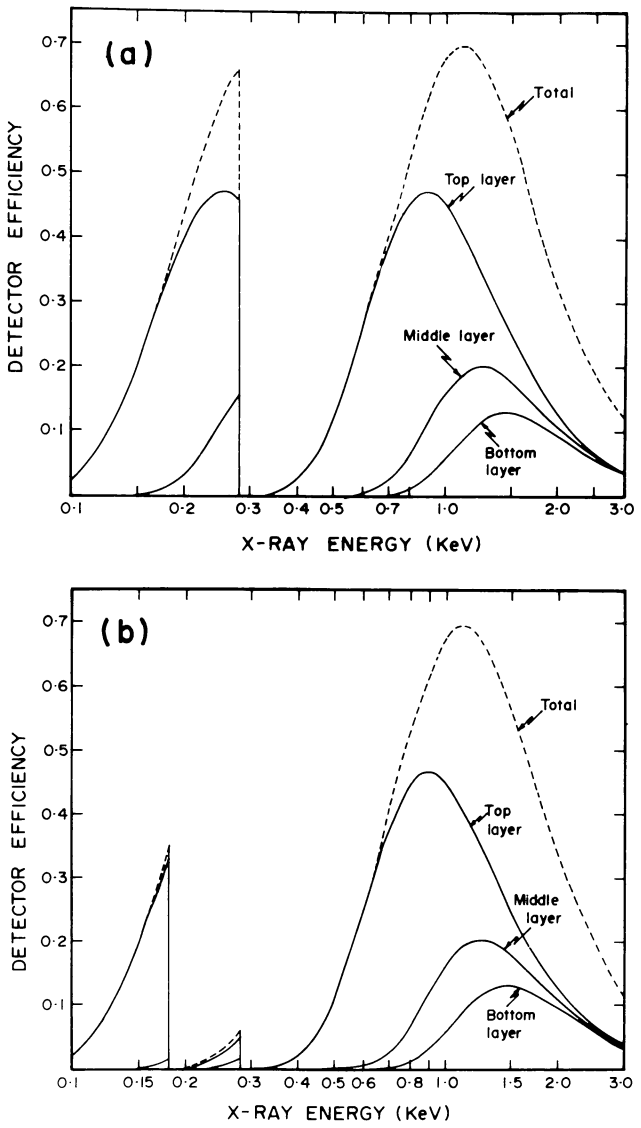

Fig. 1a and b. Detection efficiency of multi-wire proportional counter filled with pure propane gas at pressure of 200 Torr and carrying 1.5 μ thick polypropylene windows coated **a** with carbon (thickness = 35 μg cm^{-2}), **b** with boron (thickness = 70 μg cm^{-2})

2. Experiment

The observations were made with two rocket borne proportional counters. The two 4-layered (16 anodes/layer), wire-wall, gas-flow proportional counters were arranged in a back-to-back geometry. Each counter had a complete three-sided wall anti-coincidence shield for charged particle rejection. The odd and even cells of the top three layers were operated in anti-coincidence with each other to reduce the non-cosmic X-ray background. Each counter had an effective area of 495 cm^2 with a polypropylene window of 1.5 μ thickness. One counter window was coated with 35 μg cm^{-2} of carbon and the other was coated with 70 μg cm^{-2} of boron. The counters were filled with propane gas at a pressure of 200 Torr. The pressure inside the counters was maintained steady at 200 Torr by an on-board gas control system. Figure 1 shows the detection efficiency of the counters as a function of photon energy. The energy resolution of the counters, ΔE (FWHM)/E, was 85% at 0.28 keV and 38% at 1.5 keV. Both the counters had identical fields of view defined by aluminium slat collimators to 5° × 5° (FWHM). Further details of the payload are described in Singh et al. (1980).

The rocket was launched from Sriharikota Range in India (SHAR: lat. = 13°.7 N, long. = 80°.2 E, and geomag. lat. = 5°.2 N) at 1706 h. UT on June 24, 1979. Three mutually perpendicular magnetometers, coaligned with the X-ray detectors provided the aspect at any given instant. The rocket was allowed to precess with a half-cone angle of 34°. The spin period stabilised at 0.68 s and the precession period at 58.5 s. The rocket reached an apogee of 332 km and spent 400 s above the altitude of 150 km. Inflight calibration of the proportional counters was provided by 1.5 keV Al-K fluorescent X-ray line, once every 100 s.

3. The data

The experiment surveyed nearly half the sky in the northern and southern galactic hemispheres. Counts in L (0.1–0.28 keV), B (0.1–0.19 keV), and M (0.4–0.9 keV) bands, observed along the scan path were folded in each 5° × 5° sky bin in galactic coordinates corresponding to the central axis of the filed of view. The aspect solution was cross-correlated with Cen X-3/MSH 11-54 (l = 292°, b = 0°.36) which was seen as a point source in each of the precession cycle at energies > 0.5 keV. Only data obtained during the altitude range 150–330 km were analysed so that corrections due to the atmospheric absorption were negligible. Data obtained during the inflight energy calibration cycle of the detectors were discarded. Contributions from discrete X-ray sources are however, not subtracted from the X-ray brightness maps but are not significant in the L- and B-band maps.

The L and M-band intensity distribution maps (Figs. 2 and 3), in the Aitoff and Polar equal area projections, were constructed from data obtained with the counter A (with carbon coated window). The B-band intensity distribution map (Fig. 4), in the Polar equal area projection of the northern galactic hemisphere, was produced from the data obtained with the counter B (with boron coated window). There was some indication of contamination of X-ray data from counter B with UV radiation from certain regions of the sky. Such data were discarded in the analysis. From the ratio of counts in the top layer to that in the bottom two layers, the contamination due to low energy electrons was estimated to be 16.5 ± 5% in the energy intervals 2.0–2.6 keV and less than 5% for the lower energy data. In deriving the energy spectrum the data were corrected for (i) non-cosmic X-ray background; (ii) electron contamination, and (iii) the extragalactic X-ray background represented by the extrapolation of power law spectrum $11\,E^{-1.4}$ photons (cm^2 s^{-1} sterad keV)$^{-1}$ to lower energies.

The exposure of proportional counters over the celestial sphere was highly non-uniform and varied by a factor ~5. The statistical significance of intensities shown in the X-ray distribution maps is given in Table 1.

4. The spatial distribution of X-ray brightness

The soft X-ray sky maps presented here contain observations from a part of the sky bounded by l = 180° to 270° and b = 40° to 80°. This region of the sky is not so well studied in other surveys. The average X-ray brightness in the L-band (Fig. 2) shows a clear increase towards the north galactic pole by a factor ~3 to 5 than

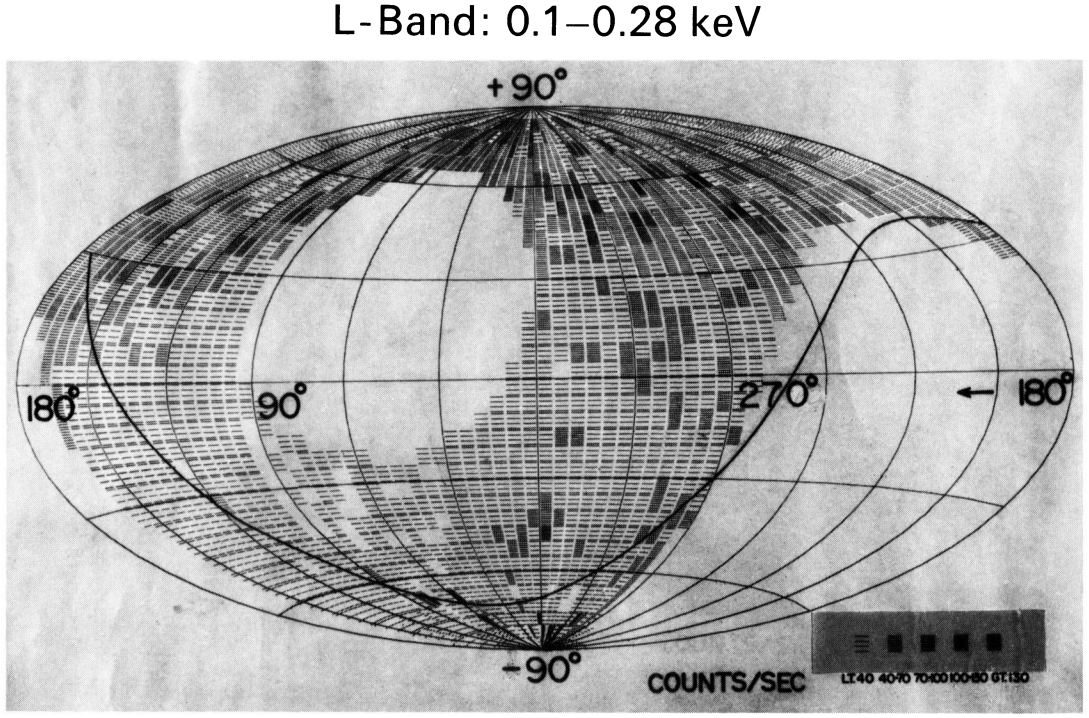

a

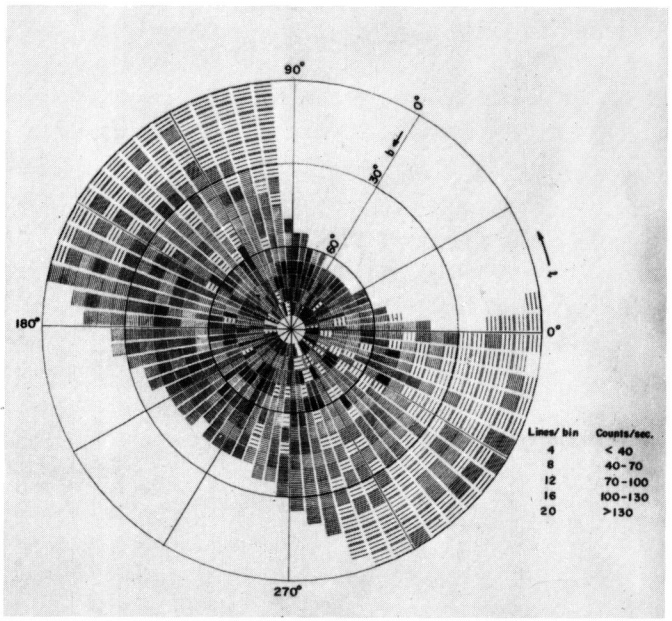

b

Fig. 2. a *L*-band (0.1–0.28 keV) X-ray brightness map in galactic coordinates (AITOFF projection). Thick line demarcates the earth's shadow. **b** *L*-band (0.1–0.28 keV) X-ray brightness map in northern galactic hemisphere (Polar projection)

that observed in the galactic plane. Also there are several regions where the soft X-ray brightness is significantly enhanced compared to the surrounding regions. Many of these regions appear to be associated with structures seen in neutral hydrogen (21 cm surveys of Fejes and Wesselius, 1973; Heiles and Jenkins, 1976), non-thermal radio continuum (Berkhuijsen, 1971; Landecker and Weilebinski, 1970), and H_α filaments (Elliot, 1970) etc. as shown in polar projection in Fig. 5 for comparison.

Table 1. Statistical significance of X-ray intensity maps

Band	Fraction of the total sky		Fraction of the surveyed sky	
	$\geqq 2\sigma$	$\geqq 3\sigma$	$\geqq 2\sigma$	$\geqq 3\sigma$
L	0.40	0.25	0.80	0.48
M	0.25	0.10	0.48	0.19
H	0.30	0.13	0.59	0.26

a) The Loop I region

A large region bounded by $l=270°$ to 30° (towards the galactic centre), $b=0°$ to 75° shows up prominently in the *M*-band maps (Fig. 3). This region contains a large portion of the Loop I (North Polar Spur) with its centre at a distance of 130 ± 75 pc (Mathewson and Ford, 1970; Iwan, 1980) and whose diameter is $\sim 230\pm135$ pc (Berkhuijsen, 1973). X-ray enhancement from inside the Loop I has been observed earlier by Hyakawa et al. (1977), Davelaar et al. (1979), Iwan (1980) and others. Present data show considerable soft X-ray excess in the *L*-band all along the inner edge of the Loop I from l, $b=270°$, 40° to l, $b=300°$, 70°. This limb brightening effect is also observed in the *B*-band at somewhat lower galactic latitude and more towards the inside of the Loop I. Enhanced diffuse X-ray emission in the *M*-band is observed from a region between $300°<l<330°$ and $-45°<b<-10°$, which is spatially coincident with the geometrical extension of Loop I in the southern galactic hemisphere. Excess X-ray emission from this region was earlier reported by Hayakawa et al. (1977) and is also seen in the X-ray maps of Fried et al. (1980). The

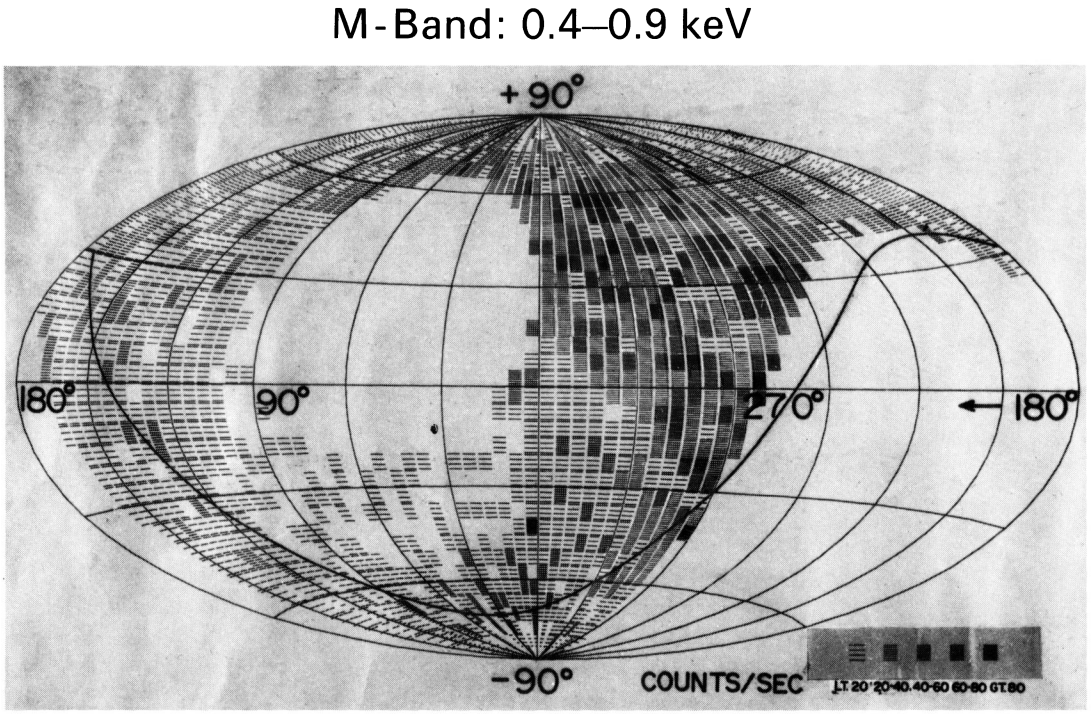

a

M-Band (0.4–0.9 keV)

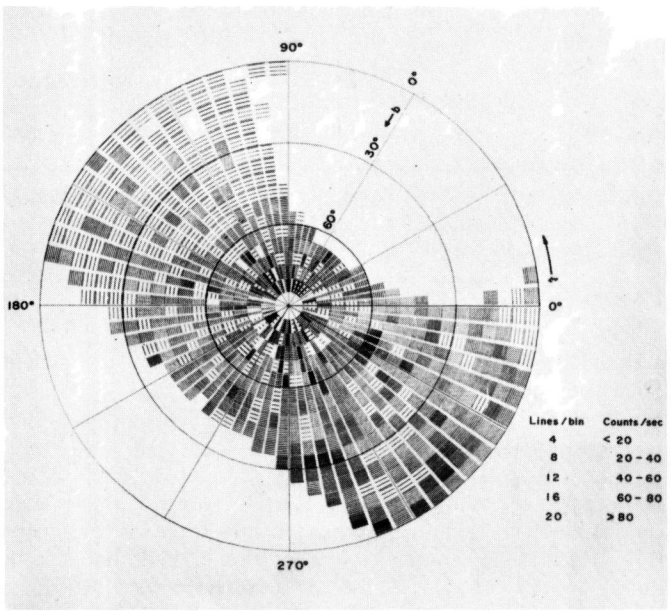

b

Fig. 3. a *M*-band (0.4–0.9 keV) X-ray brightness map in galactic coordinates (AITOFF projection). Thick line demarcates the earth's shadow. **b** *M*-band (0.4–0.9 keV) X-ray brightness map in northern galactic hemisphere (Polar projection)

Boron Band (0.1–0.2 keV)

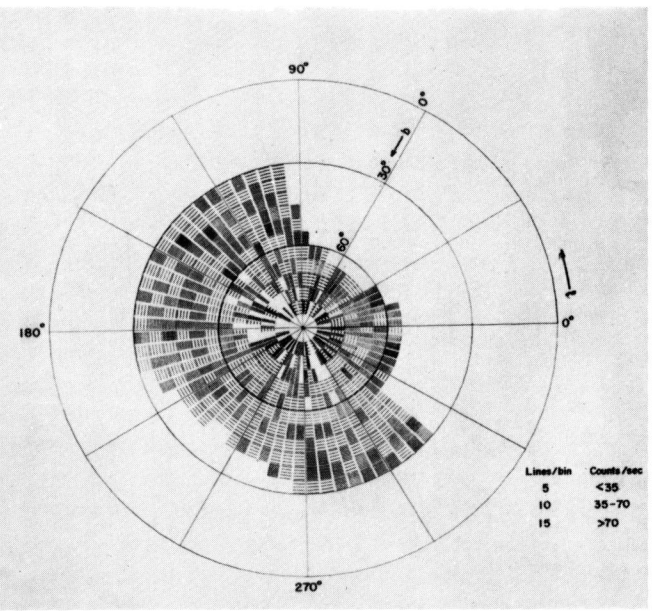

Fig. 4. *B*-band (0.1–0.19 keV) X-ray brightness map in the northern galactic hemisphere (Polar projection)

soft X-ray observations presented here, almost complete the picture of Loop I as one large circular object in the soft X-ray sky.

The situation is however, quite different in the radio continuum and 21-cm observations. The boundary of Loop I at $l=265°$, $b=35°$ to 45° is observed in the radio continuum survey (Berkhuijsen, 1971) but its association with a well defined H I ridge is controversial (Fejes and Wesselius, 1973; Heiles and Jenkins, 1976). The southern extension of Loop I, not observed in most of the radio continuum surveys except that of Yates (1968), is physically associated with a low velocity ($-20<V<30\,\mathrm{km\,s^{-1}}$) hydrogen filament and the direction of the optical polarisation vectors. A sharp increase in the polarisation at 115 pc towards the

southern extension of Loop I is in agreement with the distance of Loop I in the northern galactic hemisphere (Cleary et al., 1979).

The Loop I is a supernova shell, produced by the explosion of one of the members of Sco–Cen association inside a bubble of gas and dust formed due to strong stellar winds from early type stars of the association (Weaver, 1979). As the supernova exploded into a hot, uniform and low density medium (Hayakawa et al., 1979) the shell produced is large and highly spherical. The X-ray emission that we observe originates from the shock-heated, high temperature ($\gtrsim 3\,10^6$ K) tenuous plasma produced by the supernova explosion. Such a high temperature is necessary to explain the hard X-ray spectra observed from inside the Loop I (see Sect. 8). Iwan (1980) has suggested Loop IV as an energetic event – most probably a supernova explosion, that has reheated the Loop I. Excess diffuse X-ray emission is seen towards the Loop IV region but at present it is difficult to separate the effects of Loop I and Loop IV.

b) The Loop III and other regions

Most of the X-ray emission observed from the Loop III region, contained in our survey, is very soft (*L* and *B*-bands only). There is an increase in the X-ray intensity towards the higher latitudes inside the Loop III region. However, this X-ray emission could be part of the foreground emission.

A small region near the celestial pole and inside the Loop III region known as the "polar feature" is characterised by deficiency of radio emission in Berkhuijsen's 820 MHz survey. One of the major filaments in Heiles and Jenkins 21-cm survey is associated with it. From the associated radio continuum polarization at 1410 MHz (Spoelstra, 1972), Heiles and Jenkins have suggested that because of the lack of emission in either 21-cm or radio continuum from inside, the structure is probably filamentary rather than being an edge-on shell of a typical supernova explosion. We have discovered an excess in the *L*-band X-ray intensity at 2.8σ level from the sky bins through which the boundary of the polar feature passes. An excess *M*-band intensity is also observed in one of the sky bins inside the polar feature. However, a more sensitive survey with a finer spatial resolution is required to confirm our observations.

A prominent hole in the distribution of H I column density (Heiles, 1975) known as the Northern hole, where the N_H drops sharply to $5\,10^{19}$ atoms cm^{-2} from $1.5\,10^{20}$ atoms cm^{-2} outside the hole, is shown in Fig. 5. We have observed a significant *L*-band excess from this region and also an indication of *M*-band excess from the inside lower edge of the hole.

A large low-brightness region defined by $95° < l < 130°$, $-45° < b < 0°$ is observed in the *L*-band sky map. This overlaps with a low intensity region centered at $l, b = 110°, -30°$ with a radius of 30°, observed by Fried et al. (1980). The N_H is reported to be $\gtrsim 4\,10^{20}$ atoms cm^{-2} for this entire region (Heiles, 1975).

Our *L*-band map is in fair agreement with that of previous surveys. However, a comparison of our *M*-band map with that of de Korte et al. (1976) and McCammon et al. (1979) shows that although the two maps are quite similar in the region $300° < l < 360°$, $0° < b < 45°$ the region in the southern hemisphere for $b \gtrsim -15°$ and $330° < l < 360°$ seen brightly in their maps is not observed to be so bright in our maps. A possible cause for this discrepancy is probably due to the different nature of the two detectors and due to contribution from a large number of bright discrete sources in that region. The source contamination in the *M*-band in the case of earlier experiments is likely to be enhanced because (i) *P*-10 filled detectors of Wisconsin group have nearly twice the integral efficiency in the 1–2 keV band as compared to the efficiency of our propane filled detectors, (ii) the galactic centre sources appear very weak below 1 keV due to absorption by interstellar medium but are very bright above 1 keV, and (iii) the band spill over due to finite and poor resolution of the detectors for energies less than 2 keV. In the case of de Korte et al. (1976) the difference also arises due to the larger field of view, apart from the above factors. It is estimated that source contamination in the case of *P*-10 filled detector will be nearly twice compared to our propane filled detector. This point has also been discussed by de Korte et al. (1976), Fried et al. (1980), and Nousek et al. (1982).

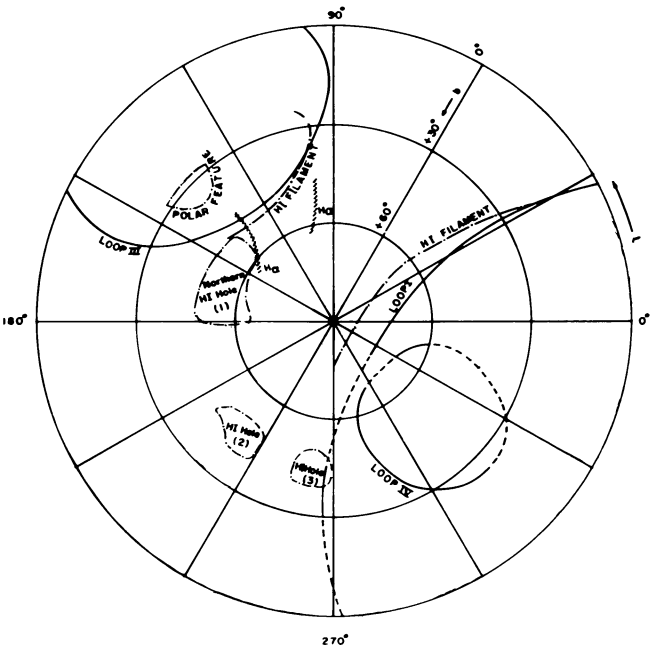

Fig. 5. Radio continuum loops (—— observed, – – – Circular extensions), neutral hydrogen (21 cm) structures –·–·–) and H_α filaments (/////) in the northern galactic hemisphere

5. Correlation of X-ray intensity with N_H

It was pointed out in Sect. 4 that a tendency for a general increase of the soft X-ray brightness is observed as N_H decreases towards the north galactic pole. The correlation plots for *L*-band intensity vs. N_H (N_H taken from Daltabuit and Meyer, 1972) for narrow latitude bands and for all longitudes in the northern galactic hemisphere are shown in Fig. 6. Each point in this diagram represents an average of counts over a bin which is 10° in longitude and 5° in latitude. Measurements with less than 3σ statistical significance are not plotted in this diagram. Typical error bars are indicated for a representative point and are normally of the order of 20% of the value in the *L*-band data. In most of the latitude bands, there is a large scatter in the *L*-band intensity for $N_H \lesssim 4\,10^{20}$ atoms cm^{-2} after which the intensity is seen to drop off very slowly. The decrease in the *L*-band intensity with increasing N_H is particularly noticeable for the latitude range of 20° to 50°. Since optical depth for photoelectric absorption in the *L*-band corresponds to $N_H \sim 2\,10^{20}$ atoms cm^{-2} where no decrease in intensity is observed, simple photoelectric absorption cannot account for the observed anti-correlation of the *L*-band

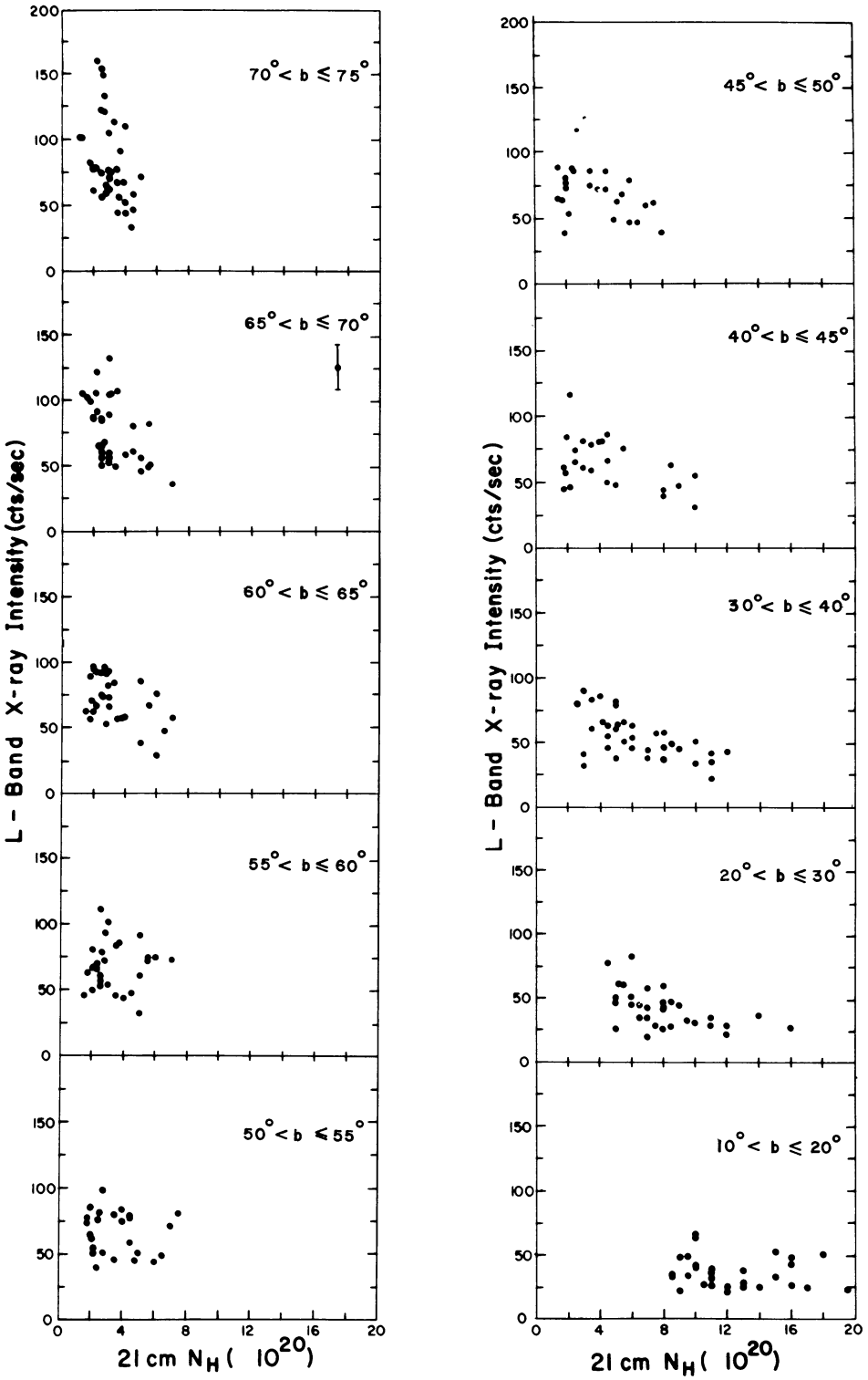

Fig. 6. *L*-band intensity vs. N_H (21 cm) for several latitude bands in the northern galactic hemisphere

intensity with N_H. A similar analysis for the southern galactic hemisphere by Sanders et al. (1977) led to the same conclusion.

The *B*-band (0.1–0.19 keV) X-rays vs. N_H plot is shown in Fig. 7. The *B*-band data is available only for the latitude range of 40° to 75°, where the contamination by UV radiation is negligible. The statistical errors are more than the errors for the *L*-band data due to lesser exposure and lower detector efficiency in this band. The error bars have been indicated for a few points. The data from regions inside and outside the NPS are shown separately because the excess X-ray emission from NPS is superposed over the foreground emission in the NPS direction. The *B*-band intensity is observed to decrease with increase in N_H for the regions outside NPS. The intensity drops off slowly at $N_H \sim 2.5\,10^{20}$ atoms cm^{-2} before which it is almost constant with a large scatter. The optical depth for photoelectric absorption in the *B*-band corresponds to $N_H \sim 10^{20}$ atoms cm^{-2}. Therefore the observed anti-correlation

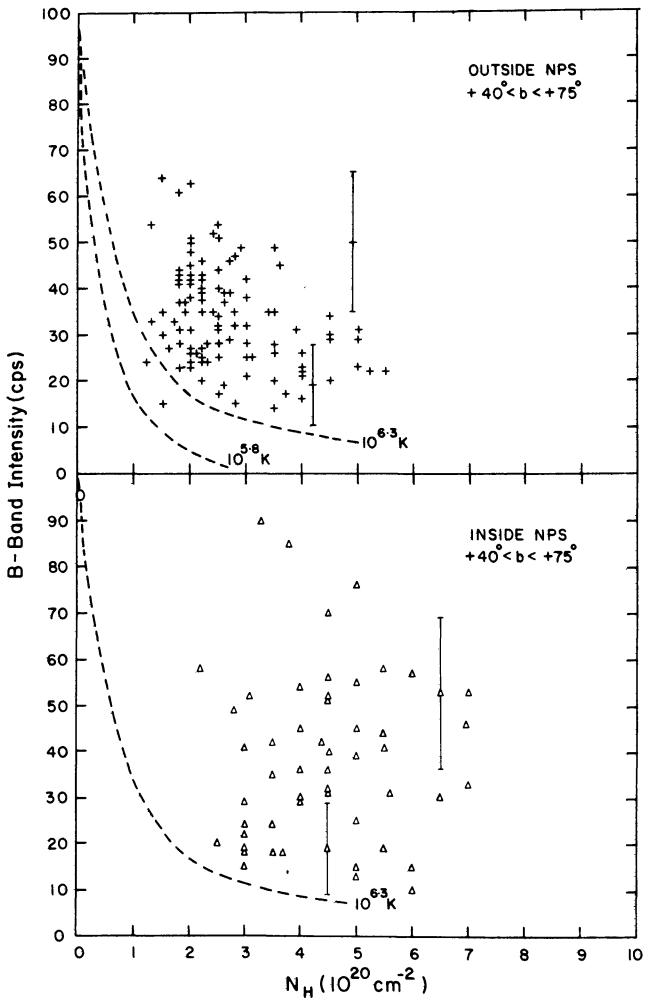

Fig. 7. *B*-band intensity vs. N_H for regions inside and outside the Loop I (North Polar Spur – NPS). The curves drawn represent the values predicted by Kato plasma with absorption by N_H. Temperature of the plasma is indicated in the figure

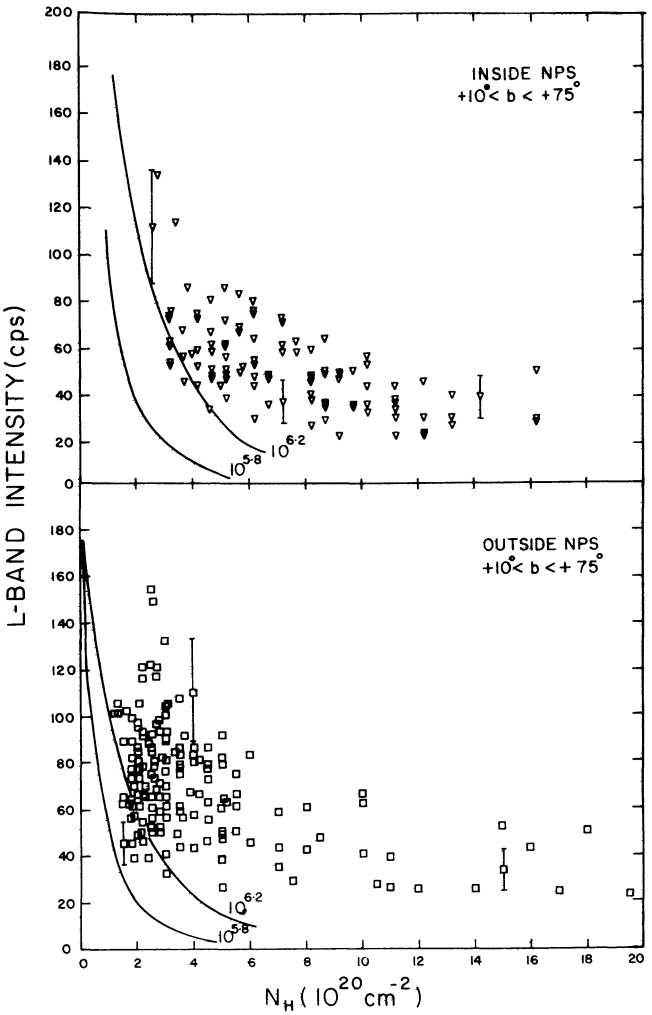

Fig. 8. *L*-band intensity vs. N_H for regions inside and outside the Loop I. The curves drawn represent the values predicted by Kato plasma with $T=10^{5.8}$ K, $10^{6.2}$ K and with absorption by N_H in the line of sight

cannot be explained by the photoelectric absorption. Similar plot of the *L*-band intensity vs. N_H is shown in Fig. 8, showing the same trends as observed in Fig. 7. The average *L*-band intensity is higher outside the NPS than inside it indicating that there is some neutral matter between us and the NPS.

Using the calculation of Kato (1976) for X-ray emission from a hot, thin plasma, the simulated *L*- and *B*-band rates have been calculated for representative temperatures in the range of $10^{5.8}$ K to $10^{6.3}$ K and with simple photoelectric absorption due to different values of N_H. The predicted count rates vs. N_H curves are plotted in Figs. 7 and 8. These curves fail to describe the data, thereby indicating the lack of quantitative correlation between X-ray intensity and N_H.

The observed lack of energy dependent absorption in the *B*- and *L*-bands (Figs. 6–8) is consistent with the fact that there is very little amount of neutral material between the sun and the regions emitting soft X-rays, with the exception of the Loop I region. Corroborating evidence for very low N_H in the solar neighbourhood has also come from the Lyman-α absorption measurements towards nearby stars (Bohlin et al., 1978). For example, the stars αVir, δCen, βCen, νSco, λSco, and αPav, which are at distances of 86 pc, 84 pc, 134 pc, 102 pc, and 57 pc respectively, have n_H values of 0.038, <0.4, 0.127, <0.043, <0.076, and 0.11 cm^{-3} respectively, indicating that most of the cold material measured in 21 cm absorption must be behind the emission regions which are therefore local. The apparent anti-correlation of soft X-ray intensity in some directions can be explained as arising from a "displacement" effect (Sanders et al., 1977). The correlation plots (Figs. 6–8) could also be explained if a large fraction of cold neutral gas in the interstellar medium were clumped in optically thick clouds and interspersed in the hot plasma producing X-rays (McKee and Ostriker, 1979) with the variation in the number of such clouds resulting in the variations in the *L*- and *B*-band intensities. However, the observed spatial intensity fluctuations (Levine et al., 1979) do not support such an explanation (Fried et al., 1980).

6. Correlation between *L*- and *B*-band intensities

Using the observed *L*- and *B*-band intensities we evaluate the relationship between the extent (d) of the local hot plasma and its pressure (P) as follows:

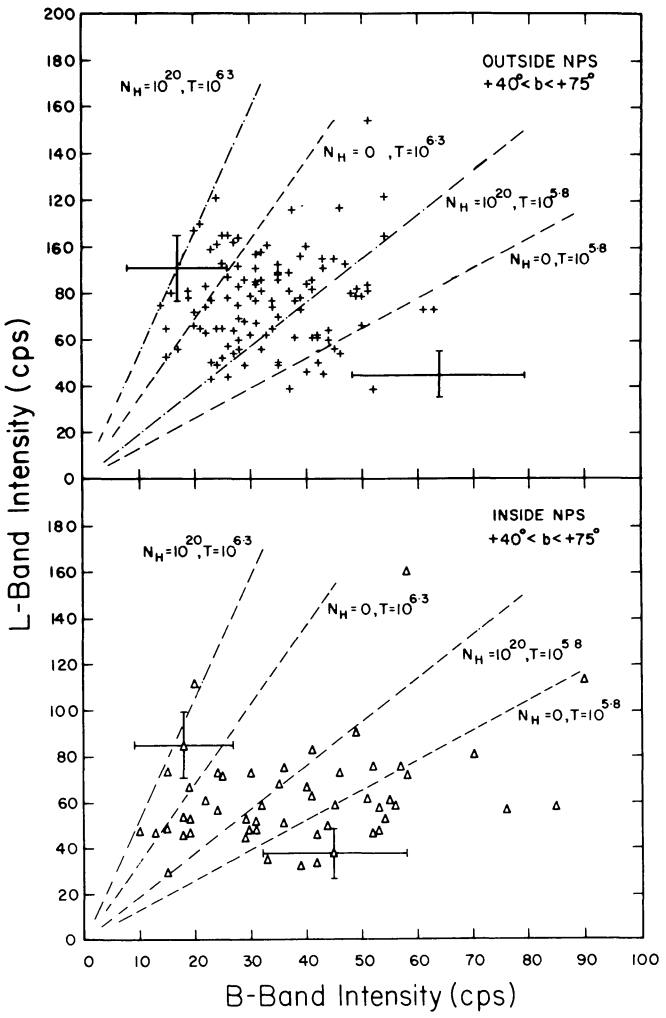

Fig. 9. *L*-band intensity vs. *B*-band intensity for the regions inside and outside the Loop I. The straight lines drawn represent the values predicted by Kato plasma with $T=10^{5.8}$ K and $10^{6.3}$ K, without interstellar absorption ($N_H=0$) and with interstellar absorption ($N_H=10^{20}$ cm^{-2})

For a hot thin plasma, the intensity of the local unabsorbed emission is given by:

$$I(E)=\frac{\Lambda(T,E)}{4\pi E}n_e^2 d, \tag{1}$$

where n_e is the average electron density and $n_e^2\Lambda(T,E)$ is the average volume emissivity of the plasma at temperature T. Since the pressure is given by $P/k=2n_eT$, we can write

$$P/k=T\left[\frac{16\pi EI(E)}{d\Lambda(T,E)}\right]^{1/2}. \tag{2}$$

Using the calculations of Kato (1976) for the X-ray emission from a hot thin plasma with cosmic elemental abundances and assuming a plasma temperature of $10^{5.9}$ K, which corresponds to spectral peaking in the *B*-band, and folding it through the response function of X-ray detection used in the RH-12A flight, the above expression integrated over *B*-band gives,

$$P/k=2.36\,10^4\left[\frac{I_B}{d}\right]^{1/2}, \tag{3}$$

where I_B is the *B*-band intensity observed [in counts (cm^2 s^{-1} sterad keV)$^{-1}$], d is in parsecs and P/k is in cm^{-3} K.

If maximum pressure is assumed to be 10^4 cm^{-3} K, then from expressions (3) one can calculate the minimum extent of such a plasma around us using the minimum value of the observed intensities in the *B*-band. The minimum *B*-band intensity observed outside the LoopI region is $\sim$9 cts (cm^2 s^{-1} sterad keV)$^{-1}$. If this intensity is due to unabsorbed emission from the plasma at $T=10^{5.9}$ K and $P/k\lesssim 10^4$ cm^{-3} K then the minimum extent (d) of the plasma required in this direction is $\sim$50 pc. A similar calculation using the *L*-band data gives a somewhat higher value ($\sim$75 pc) for the minimum extent of the plasma. Fried et al. (1981) found a minimum linear extent of the plasma to be 40 pc from a similar discussion of their data. However, Arnaud et al. (1981) have independently estimated the extent of local hot ISM to be $<$80 pc.

Figure 9 shows the *L*-band intensity plotted against the *B*-band intensity for bins of 10° × 5° (10° in l and 5° in b) for the portion of the maps where both the data exist. The maps have been divided into two parts i.e., outside and inside the Loop I. Although the statistical error indicated for a few representative points – is very large for individual points, the total scatter in the data is still larger. The ratio of *L*-band intensity to *B*-band intensity varies from $\sim$1 to $\sim$6. Straight lines drawn in the figure indicate the expected relationship between *L*- and *B*-band intensities for plasma (Kato, 1976) at temperatures $10^{5.8}$ K and $10^{6.3}$ K (i) with $N_H=0$ and (ii) with intervening $N_H=10^{20}$ atoms cm^{-2}. The maximum variation in the ratio of these intensities expected from the range of temperatures of the plasma is $\sim$3.5. Larger variations are expected due to the presence of an intervening absorber. However, even the presence of absorber column density as large as 10^{20} atoms cm^{-2} between us and the nearby plasma cannot explain the total scatter observed in Fig. 9 unless the temperature of the plasma is also made to vary from $10^{5.8}$ K to $10^{6.3}$ K. Thus, variations in the temperature and emission measure of the emitting region are required to explain the observed variations in the foreground *L*- and *B*-band emission.

A general resemblance – although not in details – is observed between the *L*- and *B*-band intensity maps (Figs. 2, 4). As the narrow *B*-band intensities are a subset of the broader *L*-band intensities (see the detector efficiency curves in Fig. 1) and since the *B*-band X-rays would be most affected by nearby cold interstellar material with $N_H\sim 10^{20}$ atoms cm^{-2}, such material will result in larger variations in the *B*-band map than in the *L*-band thus spoiling their general resemblance. Thus it is concluded that the structure seen in the soft X-ray intensity maps is due primarily to variations in the temperature and emission measures of the hot plasma rather than absorption by cold neutral interstellar material. Figure 10 shows the spatial variation of the ratio R of *L*-band to *B*-band intensity in the equal area polar projection of the northern galactic hemisphere. The ratio R is lowest for the regions very close to the northern galactic pole, indicating a very soft X-ray spectrum for the region. A decreasing ratio was observed towards the galactic plane by Burstein et al. (1977) in the region of $340°<l<360°$, $-50°<b<35°$ whereas Levine et al. (1976) in their data in the northern galactic hemisphere, near the anti-centre region, observed the X-ray energy spectrum to be softer at higher latitudes. The result here is in

agreement with that of Levine et al. There are no overlapping regions in the *B*-band maps of Burstein et al. and the present experiment. There is considerable structure seen in the polar plot of ratio *R* (Fig. 10) consistent with existence of a large variation in temperature over the observed regions.

7. Constraints on local plasma model from O VI measurements

The Copernicus measurements of O VI in the absorption spectra of early type stars show that hot gas in the temperature range of $3\,10^5$ K to 10^6 K exists in the interstellar medium (Jenkins, 1977). The O VI column densities (N_{OVI}) measured towards the direction of different stars e.g. ε Per, δ Cru, η Uma, ϕ Cen, β Cen A, and π Sco which lie on our scan paths and are at respective distances of 316 pc, 145 pc, 41 pc, 225 pc, 126 pc, and 196 pc, are $<10^{13}$ cm^{-2} (Jenkins, 1978). Taking the upper limit at 10^{13} O VI atoms cm^{-2} for distances less than 400 pc (see Fig. 4 in Jenkins, 1977) and requiring the production of minimum observed *B*-band intensity by the hot plasma, one can calculate the constraints on the model of local plasma at temperature *T*, its extent *d*, and its pressure *P*, as follows:

$$N_{OVI} = d n_{OVI} = n_e d \frac{n_H}{n_e}\frac{n_O}{n_H}\left(\frac{n_{OVI}}{n_O}\right)_T, \tag{4}$$

where n_e, n_H, n_{OVI} are the number densities of electrons, hydrogen atoms, oxygen atoms and O VI ions, respectively.

Assuming hydrogen to be completely ionised, so that $n_H/n_e = 1$ and taking cosmic abundance for oxygen (Allen, 1973), i.e. $n_O/n_H = 6.6\,10^{-4}$, we get

$$10^{13}\,\mathrm{cm}^{-2} \geqq n_e d\, 6.6\,10^{-4}\left(\frac{n_{OVI}}{n_{OVI}}\right)_T$$

or

$$n_e d \leqq \frac{4.9\,10^{-3}}{(n_{OVI}/n_O)_T}\,\mathrm{cm}^{-3}\,\mathrm{pc}. \tag{5}$$

This expression gives the maximum extent of the plasma region if n_e is known. However, we can write

$$d = \frac{(n_e d_{OVI})^2}{n_e^2 d_{x\text{-ray}}}$$

$$\therefore \quad d_{max} = \left(\frac{4.9\,10^{-3}}{(n_{OVI}/n_O)_T}\right)^2 \frac{1}{EM(T)}\,\mathrm{pc}, \tag{6}$$

where $EM(T)$ is the emission measure, as a function of temperature, required to produce the minimum observed *B*-band X-ray intensity. Using the d_{max} one can then calculate the minimum value of pressure required in the plasma, from the following expression:

$$\frac{P}{k} = 2 n_e T = 2\left[\frac{n_e^2 d}{d}\right]^{1/2} \cdot T = 2\left[\frac{EM(T)}{d}\right]^{1/2} \cdot T. \tag{7}$$

Using the values of $(n_{OVI}/n_O)_T$ given by Allen and Dupree (1969) or Shapiro and Moore (1976), and $EM(T)$ as calculated from Eq. (1) using Kato plasma code, the results of above calculations are tabulated in Table 2.

Although the O VI abundance has its maximum at $T = 10^{5.5}$ K, the range of temperature of plasma chosen in Table 2 is such that the O VI abundance is significant and also sufficient *B*-band intensity is produced in the detector. As seen from the table, for lower temperature the d_{max}'s are lower. Larger *d*'s are not admissible as they would imply too much N_{OVI}. Smaller values of *d* can be admitted but require larger pressures to maintain constant emission measures for supplying the minimum X-ray flux [see Eq. (7)]. For lower temperatures ($T < 10^6$ K) there is a significant contribution to O VI emission but the pressures required are very high, whereas at higher temperatures ($T > 10^6$ K) the pressures are not too high but then the contribution to O VI emission is negligible. However, this is based on the assumption of same plasma region contributing to both O VI emission as well as X-ray emission, which may not necessarily be true. As seen in Table 2, the requirement of producing minimum observed *B*-band emission and not exceeding the O VI column density in the same plasma implies a pressure of $\gtrsim 4600$ cm^{-3} K and extent of $\lesssim 330$ pc. However, the values of $(n_{OVI}/n_O)_T$ calculated by Jordan (1969) and Shull and Steenberg (1982) are a factor of two less than those in Table 2, as a result the d_{max} values in Table 2 increase by a factor of four and the minimum pressure values decrease by a factor of two.

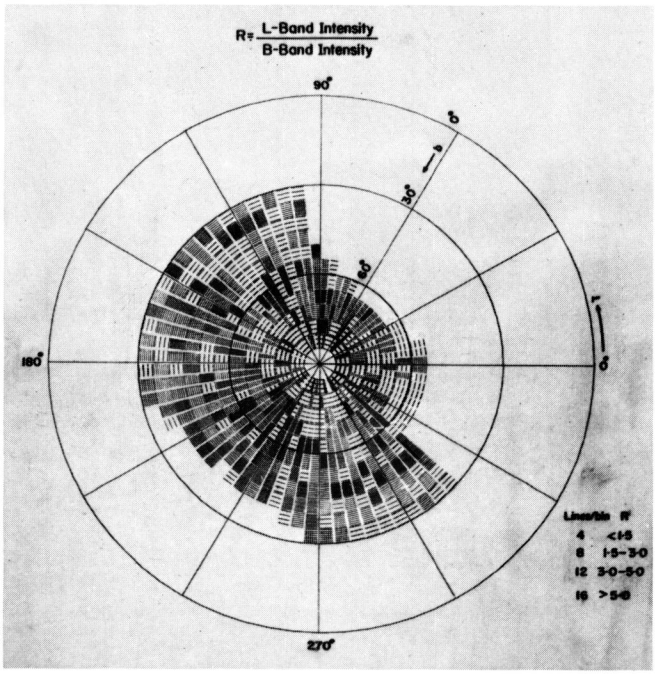

Fig. 10. Ratio of *L*-band intensity to the *B*-band intensity in the northern galactic hemisphere (Polar projection)

Table 2. Extent (*d*) and the pressure (*P*/*k*) of the local hot plasma

$\mathrm{Log}_{10}\,T$(K)	$EM(T)$ in 10^{-3} cm^{-6} pc	$(n_{OVI}/n_O)_T$	d_{max} in pc	$(P/k)_{min}$ in 10^3 cm^{-3} K
5.8	2.65	$2.46\,10^{-2}$	15	16.73
5.9	1.98	$1.15\,10^{-2}$	92	7.40
6.0	1.76	$6.46\,10^{-3}$	330	4.64
6.1	2.13	$4.47\,10^{-3}$	565	4.90
6.2	3.04	$3.40\,10^{-3}$	690	6.70
6.3	3.77	$2.19\,10^{-3}$	1330	6.73

8. Energy spectra

Energy spectra observed from a large number of very broad regions of the sky are shown in Fig. 11. Only data from counter *A* were used to derive these spectra. A single temperature, Kato plasma, with cosmic elemental abundances, convolved with our

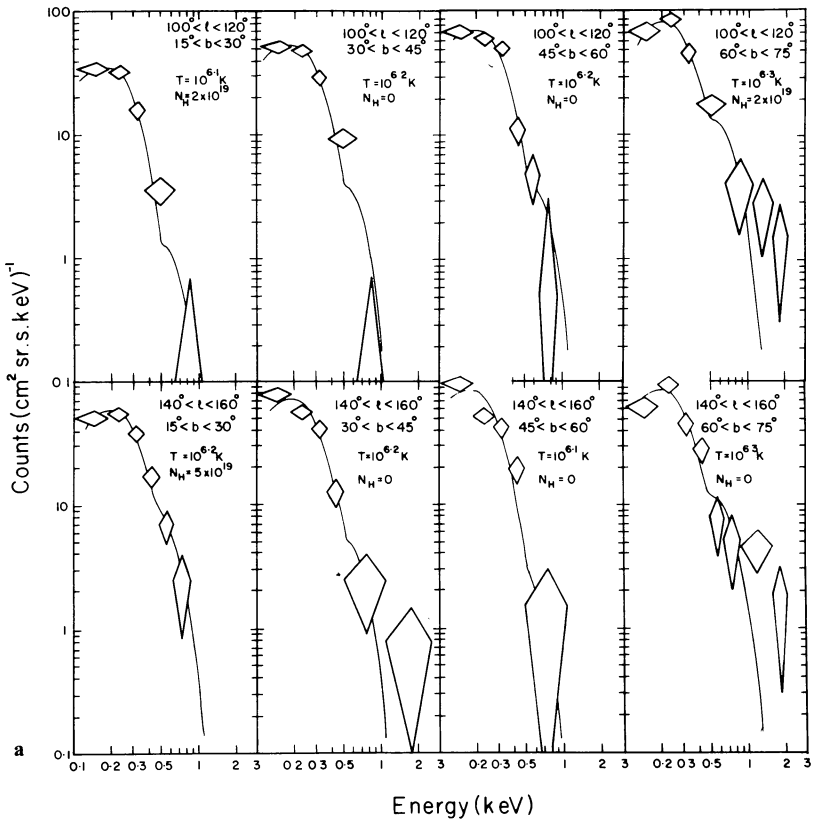

Fig. 11. a X-ray spectra from several regions of the sky in the northern galactic hemisphere. **b** X-ray spectra (continued), **c** X-ray spectra (continued)

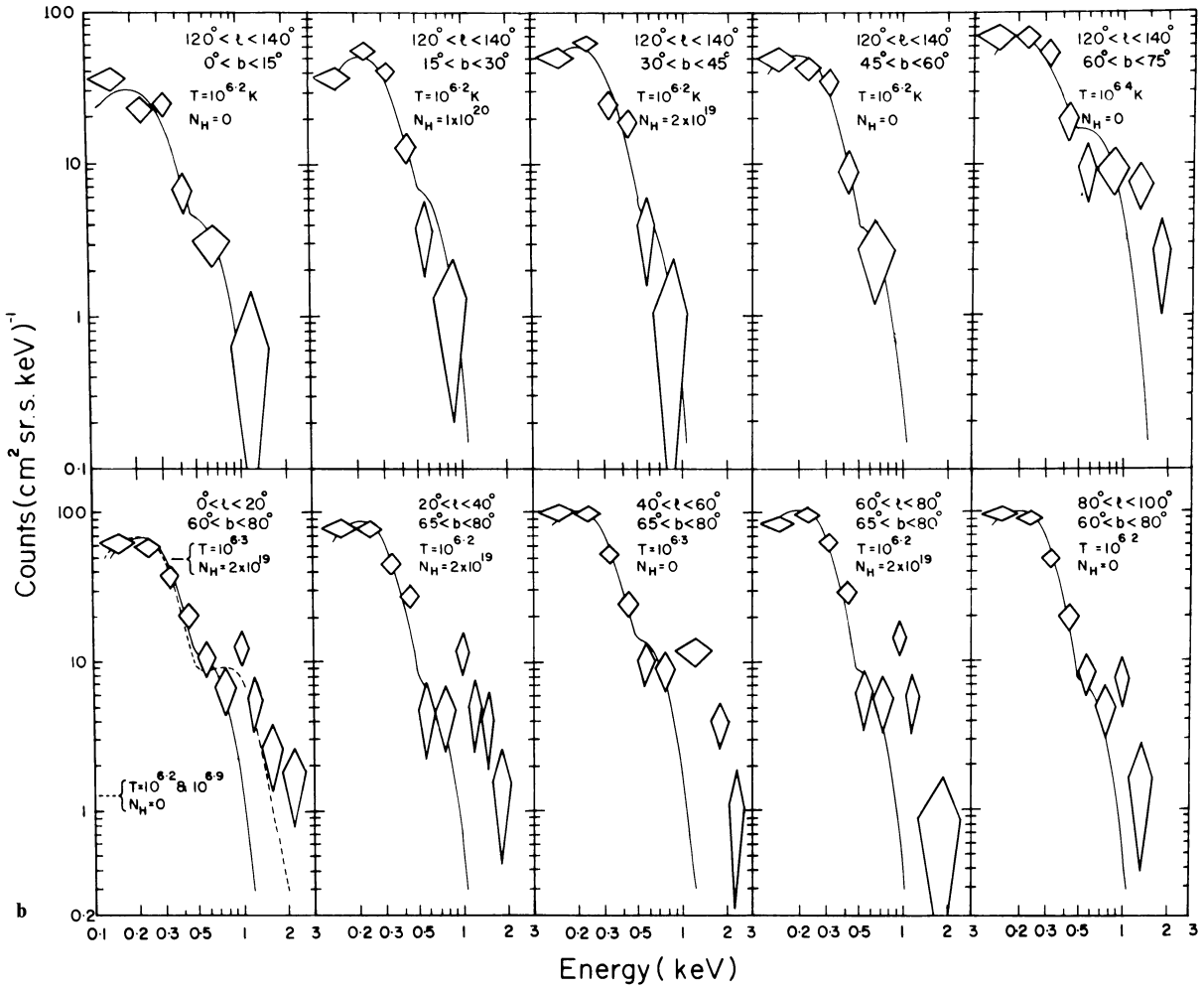

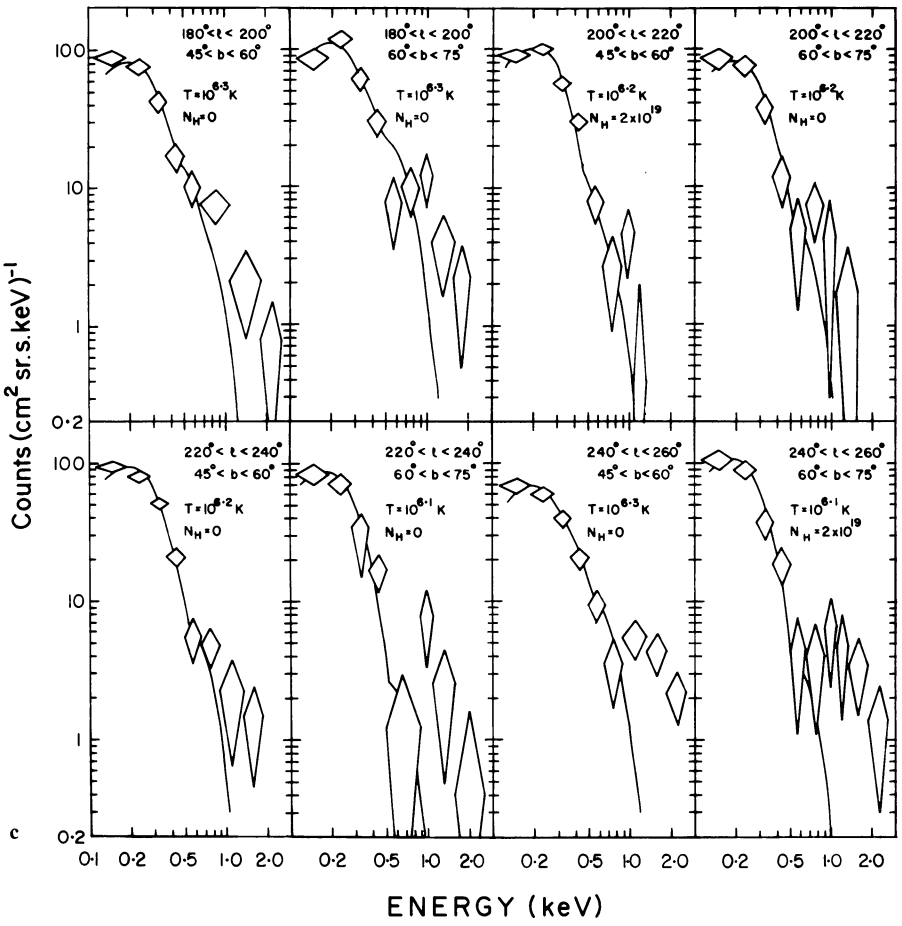

Table 3. Summary of spectral fitting data (outside Loop I region)

S. no.	Galactic longitude (deg)	Galactic latitude (deg)	χ^2_{min} (pdf)	Temperature[a] in 10^6 K	Emission measure[a] in 10^{-3} cm^{-6} pc	N_H max (10^{20} cm^{-2})	Intensity (10^{-8} erg cm^{-2} sterad^{-1} s^{-1})	
							L-band	*M*-band
1	100–120	15–30	0.55	1.6 (1.1–2.3)	2.7 (2.6–2.9)	0.8	5.9	0.7
2	100–120	30–45	0.65	2.0 (1.4–2.5)	5.0 (4.5–6.7)	0.8	7.2	1.7
3	100–120	45–60	1.375	1.6 (1.1–1.9)	5.8 (5.5–6.1)	0.9	12.4	1.5
4	100–120	60–75	0.96	2.0 (1.6–2.8)	8.2 (7.1–11.4)	1.2	11.7	2.7
5	120–140	0–15	1.74	2.0 (1.4–2.5)	3.0 (2.4–3.7)	1.1	4.3	1.0
6	120–140	15–30	2.32	2.0 (1.3–2.3)	4.9 (4.1–5.3)	1.0	7.0	1.6
7	120–140	30–45	2.12	1.6 (1.3–2.25)	4.9 (4.5–5.7)	1.5	10.5	1.3
8	120–140	45–60	0.67	1.6 (1.1–2.25)	4.3 (4.1–4.9)	1.5	9.3	1.1
9	140–160	15–30	0.96	2.0 (1.4–2.25)	5.8 (4.9–6.5)	0.8	8.3	1.9
10	140–160	30–45	1.4	1.6 (1.1–2.2)	5.9 (5.7–6.9)	1.1	12.6	1.5
11	140–160	60–75	1.8	2.0 (1.4–2.5)	8.3 (6.9–10.0)	1.5	11.9	2.7
12	180–200	45–60	1.57	2.0 (1.6–2.8)	8.0 (6.9–10.6)	0.7	11.5	2.7
13	180–200	60–75	1.77	2.0 (1.4–2.4)	10.4 (9.0–12.2)	0.7	14.8	3.4
14	200–220	45–60	1.9	1.6 (1.4–2.2)	8.8 (8.1–9.4)	1.5	19.0	2.3
15	200–220	60–75	0.78	1.6 (0.95–2.2)	6.7 (6.5–8.1)	1.2	14.4	1.7
16	220–240	45–60	1.81	1.6 (1.4–2.0)	7.7 (7.3–8.3)	0.9	16.6	2.0
17	220–240	60–75	1.19	1.3 (0.8–2.2)	6.1 (6.0–8.8)	2.0	17.6	1.1
18	240–260	60–75	1.66	1.6 (0.95–2.1)	7.7 (7.7–10.2)	1.0	16.6	2.0
19	80–100	60–80	1.70	1.6 (1.3–2.1)	8.6 (8.1–9.8)	1.0	18.5	2.2

[a] Quantities inside the bracket are the 90% confidence limits (Lampton et al., 1976)

X-ray detector was tried for fitting the data. Such a plasma was found to fit the data for a large number of regions lying outside the Loop I region. Acceptable fits as determined by χ^2 values and with reasonable values of emission measures were found only for a completely unabsorbed plasma and are summarised in Table 3. Best fit temperatures and emission measures with their 90% confidence range (Lampton et al., 1976) are listed. The source flux intensities obtained from the best fits for the *L*- and *M*-band are also derived and listed in the table. Out of the 19 regions shown in Table 3 there are nine regions which show excellent agreement ($\chi^2_{\rm pdf} \approx 1.4$) with the single temperature local plasma model (Kato, 1976). The best fit temperatures obtained for all these regions are (1.6–2.0) 10^6 K, with the 90% confidence range of temperatures for the whole set of observations in Table 3 being only (1.0–2.5) 10^6 K. The required emission measures, however, have a larger spread in their values. As a very narrow range of temperatures describes the whole set of data in Table 3 quite well, we have estimated the upper limit (at 90% confidence level) for the neutral hydrogen column density between us and the plasma by assuming that the best fit temperature for a given region in Table 3 is acceptable. These values of $N_{\rm H}$ are also listed in Table 3. However, as shown by Inoue et al. (1979), the Raymond-Smith plasma model gives higher temperature for the observed X-ray emitting regions as compared to the Kato model with the best fit temperature being higher by nearly 30%.

In all the other regions, not shown in Table 3 but for which the energy spectrum distributions are shown in Fig. 11a–c, a single temperature unabsorbed plasma model was found to be unacceptable. A two temperature model with an unabsorbed lower temperature component and a higher temperature component with variable absorption up to the maximum permitted by 21 cm radio observations improves the fit to data in these regions where single temperature model is either unacceptable or gives poor fits. However, it is very hard to find acceptable best fit parameters for two temperature model because of a large number of free parameters involved and very few data points. Therefore, we can only make a general statement that two temperature models are very likely to explain the data in many regions. A similar two temperature model ($T_1 = 10^6 - 2.5\,10^6$ K; $T_2 = 3\,10^6$–10^7 K) is required to explain the X-ray spectra from regions inside Loop I.

From a detailed spectral study of three regions viz., (l, $b = 284°$, $-80°$), (l, $b = 21°$, $42°$), and (l, $b = 70°$, $-44°$), and the similarity of the energy spectra in other regions in the southern galactic hemisphere, Nousek (1978) concluded that a two temperature plasma model of Raymond and Smith (1977) with temperatures of $\sim 10^{6.1}$ K and $\sim 10^{6.5}$ K describes the foreground X-ray emission adequately. Hayakawa et al. (1978) from their spectral analysis of 12 regions in the sky, along the galactic longitudes 150° and 330°, reached the conclusion that a single temperature Kato plasma is sufficient to describe the foreground X-ray emission. From the spectral analysis of a large number of regions in the sky we find that although a single temperature ($T \cong 10^{6.2}$ to $10^{6.3}$ K) plasma model is sufficient to describe the diffuse X-ray emission from certain regions of the sky, there exist several other regions in the sky where a two temperature plasma model would be more suitable for describing the spectral data.

9. Conclusions

The results of our sky survey of diffuse emission in soft X-rays in *B*, *L*, and *M* energy bands can be summarised as follows:

(a) A very patchy distribution of *L*-band X-rays is observed over the sky surveyed which includes a part of the sky ($180° < l < 270°$, $40° < b < 80°$) not covered in the otherwise complete survey of Wisconsin.

(b) Limb brightening along the inside edge of Loop I from l, $b = 270°$, $40°$ to l, $b = 300°$, $70°$ has been observed in the *L*- and *B*-bands. Excess soft X-ray emission in *L*-band has also been observed from the northern H I hole and is indicated along the edge of a "polar feature".

(c) The southern extension of the Loop I is observed in *M*-band sky map. Enhanced X-ray emission in the *M*-band is also observed from inside the Loop I in the northern galactic hemisphere and is indicated inside the "polar feature".

(d) A lack of quantitative correlation between the X-ray intensity and $N_{\rm H}$ is observed. The present data are explained by the displacement effect of a local hot plasma or emission from a hot plasma containing interpersed clouds.

(e) A spread in the temperature ($10^{5.8}$–$10^{6.3}$ K) of the hot plasma with cosmic elemental abundance can explain the observed variation in the *L*-band to *B*-band hardness ratio. The hardness ratio is observed to decrease towards the northern galactic pole, indicating a very soft spectrum in the polar region.

(f) X-ray spectra have been obtained with counter *A* from a large number of broad regions outside Loop I. Some of these are found to fit well with the thermal emission spectra of a hot plasma with cosmic elemental abundances and negligible interstellar absorption. The best fit temperature of the local plasma required is $10^{6.2}$–$10^{6.3}$ K. A second higher temperature component of the plasma improves the fit to the observed spectra in some other regions. The emission measures of the plasma obtained from the observed X-ray spectra of a large number of regions is found to vary from region to region in the range (0.27–1.0) 10^{-2} cm^6 pc.

(g) The requirement of producing the minimum observed *B*-band emission without exceeding the O VI column density in the same plasma implies a pressure of $\gtrsim 4600\,{\rm cm}^{-3}$ K and extent of $\lesssim 330$ pc for the plasma.

Acknowledgements. We are grateful to the Indian Space Research Organisation for the allotment of an RH-560 rocket, the payload integration staff of Thumba Equatorial Rocket Launching Station, Trivandrum for payload support and the ground support staff at SHAR for the excellent launch. We thank Messrs. J. Rodrigues, J. A. D'Silva, M. R. Shah, S. S. Mohite, and N. V. Bhagat for technical help. We thank Shri A. V. John for assistance in the computer programming. Our thanks are due to Dr. T. Kato of Institute of Plasma Physics, Nagoya, Japan for providing us the thermal plasma code.

References

Allen, J.W., Dupree, A.K.: 1969, *Astrophys. J.* **155**, 27
Allen, C.W.: 1973, Astrophysical Quantities, (3rd ed.) Univ. of London
Arnaud, M., Rocchia, R., Rothenflug, R., Soutoul, A.: 1981, 17th ICRC, XG 1, 131
Berkhuijsen, E.M.: 1971, *Astron. Astrophys.* **14**, 359
Berkhuijsen, E.M.: 1973, *Astron. Astrophys.* **24**, 143
Burstein, P., Borken, R.J., Kraushaar, W.L., Sanders, W.T.: 1977, *Astrophys. J.* **213**, 405
Cleary, M.N., Heiles, C., Haslam, C.G.T.: 1979, *Astron. Astrophys. Suppl.* **36**, 95
Cox, D.P., Smith, B.W.: 1974, *Astrophys. J. Letters* **189**, L 105
Cox, D.P.: 1979, *Astrophys. J.* **234**, 863
Cox, D.P.: 1981, *Astrophys. J.* **245**, 534
Daltabuit, E., Meyer, S.: 1972, *Astron. Astrophys.* **20**, 415

Davelaar, J., Bleeker, J.A.M., Deerenberg, A.J.M., Tanaka, Y., Hayakawa, S., Yamashita, K.: 1979, *Astrophys. J.* **230**, 428
de Korte, P.A.J., Bleeker, J.A.M., Deerenberg, A.J.M., Hayakawa, S., Yamashita, K., Tanaka, Y.: 1976, *Astron. Astrophys.* **48**, 235
Elliot, K.H.: 1970, *Nature* **226**, 1236
Fejes, I., Wesselius, P.R.: 1973, *Astron. Astrophys.* **24**, 1
Fried, P.M., Nousek, J.A., Sanders, W.T., Kraushaar, W.L.: 1980, *Astrophys. J.* **242**, 987
Hayakawa, S., Kato, T., Nagase, F., Yamashita, K., Murakami, T., Tanaka, Y.: 1977, *Astrophys. J. Letters* **213**, L 109
Hayakawa, S., Kato, T., Nagase, F., Yamashita, K., Tanaka, Y.: 1978, *Astron. Astrophys.* **62**, 21
Hayakawa, S., Kato, T., Nagase, F., Yamashita, K.: 1979, *Publ. Astron. Soc. Japan* **31**, 71
Heiles, C.: 1975, *Astron. Astrophys. Suppl.* **20**, 37
Heiles, C., Jenkins, E.B.: 1976, *Astron. Astrophys.* **46**, 333
Inoue, H., Koyama, K., Matsuoka, M., Ohashi, T., Tanaka, Y., Tsunemi, H.: 1979, *Astrophys. J. Letters* **227**, L 85
Inoue, H., Koyama, K., Matsuoka, M., Ohashi, T., Tanaka, Y., Tsunemi, H.: 1980, *Astrophys. J.* **238**, 886
Iwan, D.: 1980, *Astrophys. J.* **239**, 316
Iwanami, H., Kuneida, H., Nagase, F., Yamashita, K., Murakami, T.: 1979, *Astrophys. Space Sci.* **61**, 217
Jenkins, E.B.: 1977, Topics in Interstellar Matter, ed. Hugo van Woerden, Reidel, Dordrecht
Jenkins, E.B.: 1978, *Astrophys. J.* **219**, 845
Jordan, C.: 1969, *Monthly Notices Roy. Astron. Soc.* **142**, 501
Kato, T.: 1976, *Astrophys. J. Suppl.* **30**, 397
Lampton, M., Margon, B., Bowyer, S.: 1976, *Astrophys. J.* **208**, 177
Landecker, T.L., Wielebinski, R.: 1970, *Australian J. Phys. Suppl.* **16**, 1
Levine, A., Rappaport, S., Doxsey, R., Jernigan, G.: 1976, *Astrophys. J.* **205**, 215
Levine, A., Rappaport, S., Halpern, J., Walter, F.: 1977, *Astrophys. J.* **211**, 215
Long, K.S., Agrawal, P.C., Garmire, G.P.: 1976, *Astrophys. J.* **206**, 411
Mathewson, D.S., Ford, V.L.: 1970, *Mem. Roy. Astron. Soc.* **74**, 139
McCammon, D., Bunner, A.N., Coleman, A.L., Kraushaar, W.L.: 1971, *Astrophys. J. Letters* **168**, L 33
McCammon, D., Meyer, S.S., Sanders, W.T., Williamson, F.O.: 1976, *Astrophys. J.* **209**, 46
McCammon, D., Kraushaar, W.L., Sanders, W.T., Burrows, D.N.: 1979, Proc. 16th ICRC, Kyoto, Japan
McKee, C.F., Ostriker, J.P.: 1977, *Astrophys. J.* **218**, 148
Nousek, J. A.: 1978, Ph. D. thesis, Univ. 9f Wisconsin, Madison
Nousek, J.A., Fried, P.M., Sanders, W.T., Kraushaar, W.L.: 1982, *Astrophys. J.* **258**, 83
Raymond, J.C., Smith, B.W.: 1977, *Astrophys. J. Suppl.* **35**, 419
Rosner, R., Avni, Y., Bookbinder, J., Giacconi, R., Golub, L., Harnden, F.R., Maxon, C.W., Topka, K., Vaiana, G.S.: 1981, *Astrophys. J. Letters* **249**, L 5
Sanders, W.T., Kraushaar, W.L., Nousek, J.A., Fried, P.M.: 1977, *Astrophys. J. Letters* **217**, L 87
Schnopper, H.W., Delvaille, J.P., Rocchia, R., Blondel, C., Cheeron, C., Christy, J.C., Ducros, R., Koch, L., Rothenflug, R.: 1982, *Astrophys. J.* **253**, 131
Seward, F.D., Mitchell, M.: 1981, *Astrophys. J.* **243**, 736
Shapiro, P.R., Moore, R.T.: 1976, *Astrophys. J.* **207**, 460
Shull, J.M., Steenberg, M.V.: 1982, *Astrophys. J. Suppl.* **48**, 95
Singh, K.P., Manchanda, R.K., Rodrigues, J., Agrawal, P.C., Naranan, S.: 1980, *Indian J. Radio Sp. Phys.* **9**, 201
Singh, K.P., Agrawal, P.C., Manchanda, R.K., Naranan, S., Sreekantan, B.V.: 1981a, 17th ICRC Paris, XG **1**, 123 (XG 4.2-1)
Singh, K.P., Naranan, S., Sreekantan, B.V.: 1981b, 17th ICRC Paris, XG **1** (XG 4.2-2)
Spoelstra, T.A.Th.: 1972, *Astron. Astrophys.* **21**, 61
Vanderhill, M.J., Borken, R.J., Bunner, A.N., Burstein, P.H., Kraushaar, W.L.: 1975, *Astrophys. J. Letters* **197**, L 19
Weaver, H.: 1979, The Large Scale Characteristics of the Galaxy, IAU *Symp.* **84**, ed. W.B. Burton, p. 295
Yates: 1968, *Australian J. Phys.* **21**, 167